Analytical and Bioanalytical Chemistry (2023) 415:7047–7055
https://doi.org/10.1007/s00216-023-05007-9

PAPER IN FOREFRONT

Time-resolved fluorescence nanoprobe of acetylcholinesterase based on ZnGeO:Mn luminescence nanorod modified with metal ions

Lifang Gao[1] · Rong Chen[1] · Haixia Li[1] · Dan Xu[1] · Danning Zheng[1]

Received: 6 September 2023 / Revised: 6 October 2023 / Accepted: 9 October 2023 / Published online: 27 October 2023

Abstract

A novel time-resolved fluorescence nanoprobe (PBMO, PLNR-BSA-Mn^{2+}-OPD) is fabricated for the label-free determination of acetylcholinesterase (AChE). The ZnGeO:Mn persistent luminescence nanorod (PLNR) and Mn(II) are, respectively, exploited as the signal molecule and quencher to construct the PBMO nanopobe using bovine serum albumin (BSA) as the surface-modified shell and *o*-phenylenediamine (OPD) as the reducing agent. In the presence of H_2O_2, the persistent luminescence of PBMO at 530 nm is enhanced remarkably within 30 s due to the oxidation of Mn(II). H_2O_2 can react with thiocholine (TCh), which is produced through the enzymatic degradation of acetylcholine (ATCh) by AChE. The PBMO nanoprobe is successfully applied to the determination of AChE in the linear range of 0.08–10 U L^{-1}, with a detection limit of 0.03 U L^{-1} ($3\sigma/s$). The practicability of this PBMO nanoprobe is confirmed by accurately monitoring AChE contents in human serum samples, giving rise to satisfactory spiking recoveries of 96.2–103.6%.

Keywords Acetylcholinesterase · Metal ions · Persistent luminescence nanorod · Time-resolved fluorescence nanoprobe

Introduction

Acetylcholinesterase (AChE) is a serine hydrolase in neuromuscular junctions, brain synapses, and erythrocytes. The main physiological process AChE participated in is hydrolyzing neurotransmitter, acetylcholine (ATCh), thus inducing the termination of signaling transmission at cholinergic synapses and neuromuscular junctions. Acetylcholinesterase also exhibits other functions, including morphoregulation, adhesion, stress, and pathogenesis [1, 2]. The researches show that AChE is associated with cell apoptosis and even considered to be a marker under certain circumstances [3]. Acetylcholinesterase is closely related to the pathogenesis of insulin-dependent diabetes and the clinical symptoms of Alzheimer's disease [4, 5]. Therefore, accurate monitoring of AChE activities is critical to disease diagnosis and intervention.

✉ Lifang Gao
gaolf@hainmc.edu.cn

✉ Danning Zheng
chemzhengdn@hainmc.edu.cn

[1] School of Pharmacy, Hainan Medical University, Haikou 571199, China

At present, varieties of methods have been adopted to explore AChE activities, such as mass spectroscopy [6], immunoassay [7], electrochemical analysis [8], colorimetry [9], and fluorescence spectrometry [10]. Among them, mass spectroscopy requires non-portable and expensive equipment; immunoassay is lengthy and labor-intensive; electrochemical analysis usually exhibits poor preparation ability; and the colorimetry has low sensitivity. Attributed to the high sensitivity, excellent stability, simple manipulation, and fast response time, the fluorimetric methodology gains increasing attention [11]. Time-resolved fluorescence (TRF) analysis is one of the most sensitive fluorimetric methodologies due to the elimination of interference from auto-fluorescence and scattering light. The application fields of TRF analysis involves immunoassays, sensing, and bioimaging. The luminescent materials with long lifetime are applied to ensure the success of delay collection to fluorescence signals [12–14].

As a kind of emerging nanomaterials, persistent luminescence nanorod (PLNR) can store energy from excitation sources and slow release it in the form of photonic emission, providing long-lasting afterglow of several hours. Compared to organic compounds, the PLNR exhibit outstanding advantages: (i) readily available, complex synthesis processes are not required; (ii) it is possible to acquire PLNPs with

different luminous performances and morphology by tuning the host and emitter; (iii) good biocompatibility and low toxicity got through surface modification [15–17]. In general, luminescence resonance energy transfer (LRET) is utilized to give the switch signal of PLNR, in which PLNR is an energy donor and other materials are energy acceptors. The emitting light of PLNR is decreased by the energy acceptors, accompanying an analyte-inducing recovery [18]. The degree of spectral overlap affects the sensitivity of the probe, so the choice of energy receptors is particularly important [19].

Attributing to the high quenching efficiency, metal ions are widely used to develop LRET systems together with various fluorophores and phosphors. To avoid the instability of metal ion–based LRET systems developed by directly mixing in aqueous solution or anchoring on the surface of nanoparticles, researchers utilize the mesoporous silica as a template to encapsulate $ZnGa_2O_4$:Cr^{3+} and metal ions [20–23]. However, the encapsulation process is tedious, which include template synthesizing, ionic impregnation, annealing, and shell encapsulating.

In this study, a novel TRF nanoprobe based on the LRET principle is fabricated for the label-free detection of AChE, referring to as PBMO (PLNR-BSA-Mn^{2+}-OPD). We developed a novel assembly strategy for the LRET system. The PLNR is coated with bovine serum albumin (BSA) combined with Mn(II) and *o*-phenylenediamine (OPD) by a simple one-pot method. Among them, phenylenediamine derivatives are always used for probe fabrication [24, 25]. Herein, the roles of PLNR, Mn(II), and OPD are as luminescent material, quencher, and reducing agent, respectively. Bovine serum albumin as the nanocarrier provides a shell cavity for Mn(II). The shell cavity not only offers reaction space for Mn(II) and H_2O_2, but also shorten the distance between energy donor and energy receptor. We found that H_2O_2 strongly increases the TRF of PBMO at 530 nm. Therefore, the PBMO nanoprobe can be applied for the determination of H_2O_2. Thiocholine (TCh) is generated in situ during the enzymatic degradation of ATCh by AChE and able to consume H_2O_2, so the PBMO nanoprobe is successfully used for the determination of AChE and its contents in human serums are successfully detected by this probe.

Experimental section

Materials and apparatus

$Zn(NO_3)_2{\cdot}6H_2O$, GeO_2, $Mn(NO_3)_2{\cdot}6H_2O$, $NH_3{\cdot}H_2O$, *o*-phenylenediamine (OPD), and *N*-ethylmaleimide (NEM) were bought from Aladdin Reagent Company (Shanghai, China, https://www.aladdin-e.com). Glutaraldehyde (50 wt%), H_2O_2 (30 wt%), NaOH, $Na_2HPO_4{\cdot}12H_2O$, $NaH_2PO_4{\cdot}12H_2O$, $FeCl_3{\cdot}6H_2O$, Na_2SO_4, CH_3COOK, and $(NH_4)_2SO_4$ were obtained from Sinopharm Chemical Reagent Co., Ltd. (Shanghai, China, http://www.reagent.com.cn). Bovine serum albumin (BSA), lysozyme, trypsin, ALP, human serum albumin (HSA), IgG, α-globulin (α-GLB), and β-globulin (β-GLB) were purchased from Sigma-Aldrich (Milwaukee, WI, USA, https://www.sigmaaldrich.cn).

The TRF measurements and UV–Vis absorption spectra were conducted on a Spectra Max M5e (Molecular Devices Co. Ltd, USA). The morphology of PBMO PLNRs was characterized via a Jem-2100F field emission electron microscope (JEOL, Japan). X-ray photoelectron spectrometry (XPS) characterization of ZnGeO:Mn PLNR and PBMO was recorded on a Thermo Scientific™ K-Alpha™+ spectrometer. X-ray diffraction (XRD) analysis was measured on a D8 Advance powder diffractometer (Bruker, Germany). Fourier transform infrared (FT-IR) spectra were carried out with a Tensor-27 FT-IR spectrophotometer (Bruker, Germany).

Synthesis of PBMO

ZnGeO:Mn PLNR was prepared by the hydrothermal method described in our previous work [26]. Briefly, Zn^{2+} (2 mmol), Mn^{2+} (5 μmol), and concentrated HNO_3 were mixed in H_2O, and then Ge^{4+} (3 mmol) was added dropwise, while $NH_3{\cdot}H_2O$ was added to adjust pH. After continuous stirring, the resulting mixture was sealed at 220 °C for 10 h. The as-prepared ZnGeO:Mn PLNR was collected through centrifugation. ZnGeO:Mn-OH PLNR was obtained by adding 50 mg of ZnGeO:Mn PLNR to 20 mL of sodium hydroxide solution (5 mmol L^{-1}) and stirring for 24 h, then washing and dissolving in H_2O for later use. The processes for the synthesis of PBMO were as follows according to the reported literature with slight modifications [27]. Twenty-five milligrams of BSA was dissolved in 1.5 mL H_2O to obtain a suspension and 1.5 mL ZnGeO:Mn-OH PLNR (10 mg mL^{-1}) was added into it. After sonicating for 15 min and stirring for 5 min, 1.5 mL of $Mn(NO_3)_2$ aqueous solution (50 mmol L^{-1}), 25 μL of OPD (2 mol L^{-1}, in DMF), 25 μL of sodium hydroxide (2 mol L^{-1}), and 10 μL of glutaraldehyde were dropped successively into the mixture, following continuously stirring for 24 h at 40 °C. The resulting products were centrifuged at 12,000 rpm and washed with H_2O for several times.

Detection of H_2O_2

Ten microliters of H_2O_2 solution (concentrations between 4 and 100 μmol L^{-1}), 10 μL of PBMO solution (400 μg

mL^{-1}), and 80 μL of PB (10 mmol L^{-1}, pH 8.5) were mixed in a black 96-well plate with 5-min vibration at 37 °C. The TRF intensity at 530 nm was recorded with excitation at 250 nm. The luminous enhancement efficiency (q_1) was achieved from the calculation formula $q_1 = F/F_0 - 1$, in which F and F_0 were the TRF intensity of PBMO after and before the addition of H_2O_2, respectively.

Calibration plot of AChE detection

For AChE detection assay, mixtures of 10 μL ATCh (20 mmol L^{-1}), freshly prepared AChE with different activities (10 μL, 0.8 – 100 U L^{-1}), and 10 μL of phosphate buffer (PB, 10 mmol L^{-1}, pH 7.4) were incubated for 10 min at 37 °C. After that, 10 μL of H_2O_2 (300 mmol L^{-1}) was added and incubated at 37 °C for another 10 min. Finally, 10 μL of PBMO solution (750 μg mL^{-1}) and 50 μL of PB (10 mmol L^{-1}, pH 8.5) were added into the mixture and equilibrated for 5 min before fluorescence measurements. The luminous quenching efficiency (q_2) was achieved from the calculation formula $q_2 = 1 - F/F_0$, in which F and F_0 were the TRF intensity with and without AChE, respectively. To evaluate the selectivity of PBMO nanoprobe for AChE, some nonspecific enzymes, proteins, and ions were individually investigated.

Real sample analysis

The human blood samples were obtained from the Jiangyuan Hospital of Jiangsu Province and all experiments were approved by the ethics committee. The samples were centrifuged at 3000 rpm for 5 min, and then the supernatant was filtered through a 0.22-μm membrane filter to obtain human serum samples. Samples were spiked with different concentrations of AChE, following adding *N*-ethylmaleimide (NEM) and diluting for 500-fold. The prepared samples were detected according to the aforementioned steps.

Results and discussion

Characterization of PBMO

To endow superior modifiability of the ZnGeO:Mn PLNR, it is first hydroxylated. The ZnGeO:Mn-OH PLNR and BSA are well pre-mixed through hydrogen bonding in water. Glutaraldehyde is used as a cross-linking agent in the presence of Mn^{2+} and OPD to coat BSA layers on the surface of ZnGeO:Mn-OH PLNR. Under an alkaline condition, MnO and DAP produced from Mn^{2+} and OPD are simultaneously loaded in the BSA shell to form PBMO. The rod

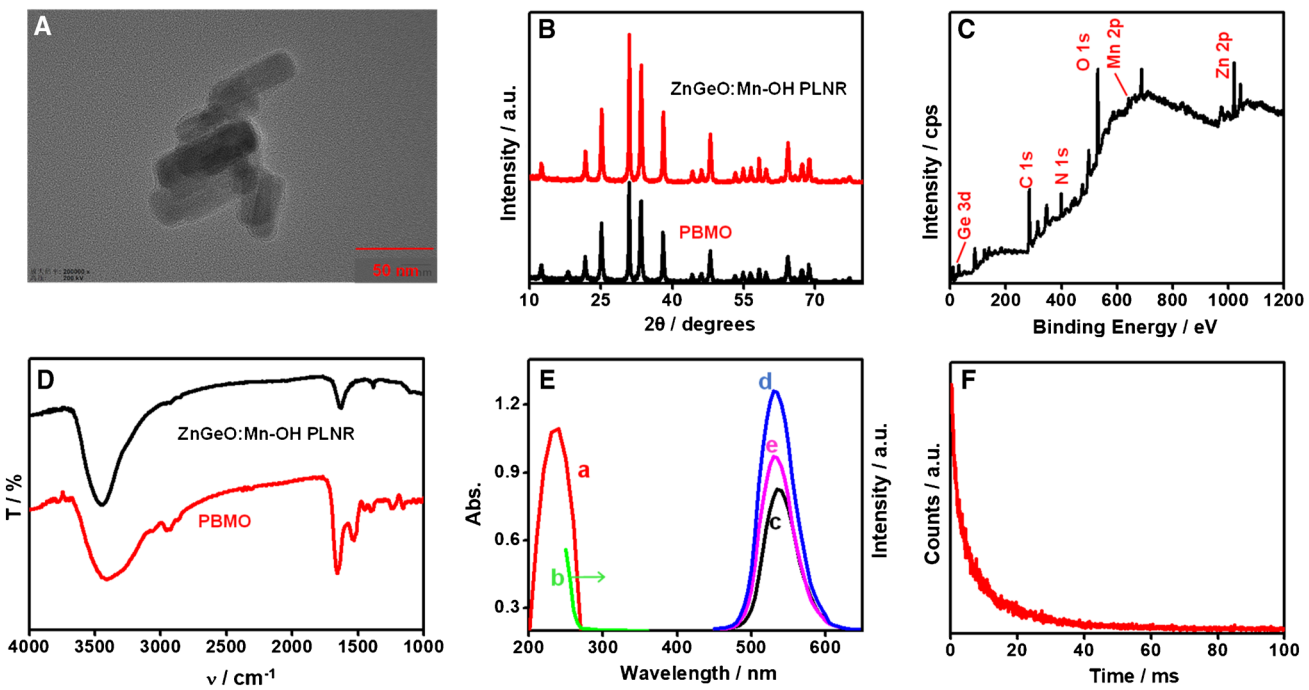

Fig. 1 **A** TEM images of PBMO. **B** Powder XRD patterns of ZnGeO:Mn-OH PLNR and PBMO. **C** XPS spectra of PBMO. **D** FT-IR spectra of ZnGeO:Mn-OH PLNR and PBMO. **E** UV–Vis absorption spectra of PBMO (a), fluorescence excitation spectra (λem = 530 nm, b) and fluorescence emission spectra (λex = 250 nm, c) of PBMO, fluorescence emission spectra of PBMO in absence of 5 μmol L^{-1} H_2O_2 (d), and fluorescence emission spectra of PBMO nanoprobe in absence of 10 U L^{-1} AChE (e). **F** Luminescence decay curve of PBMO

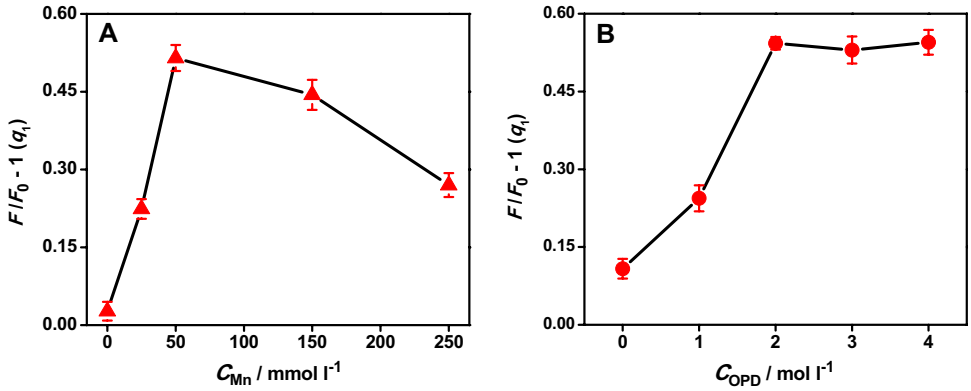

Fig. 2 The fluorescence enhancement efficiency (q_1) of PBMO prepared from different concentrations of $Mn(NO_3)_2$ (**A**) and OPD (**B**) under the addition of 5 μmol L^{-1} H_2O_2

morphology of PBMO is described in Fig. 1A. There is a uniform core–shell nanostructure, and the length and diameters of PBMO are 56.3 ± 3.1 and 22.3 ± 2.2 nm, with a shell thickness of 3.9 ± 0.6 nm.

The X-ray diffraction (XRD) results show that the XRD pattern of PBMO matched quite well with ZnGeO:Mn-OH PLNR (Fig. 1B), indicating there are no changes of the crystallization after BSA modification. The XRD patterns of PBMO are well-matched to the standard card (JCPDS No.11–0687), which is the crystallization of the rhombohedral phase [28].

In addition, X-ray photoelectron spectroscopy (XPS) spectra of PBMO (Fig. 1C and Fig. S1) exhibit typical peaks due to the presence of Zn at 1021.1 eV, Ge at 31.7 eV, Mn at 641.1 eV, C at 284.8 eV, N at 399.5 eV, and O at 530.7 eV, which relative atomic percentages are 4.49%, 6.53%, 1.62%, 50.79%, 10.57%, and 26.01%, respectively.

After coating hydroxyl-functionalized PLNR with BSA shell, PBMO shows several new absorption bands. The appearance of a broad peak at 3410 cm^{-1} along with a weak peak at 3250 cm^{-1} corresponding to the $–NH_2$ group of DAP in Fourier transform infrared (FT-IR) spectra (Fig. 1D). The peaks at 1531 cm^{-1}, 1657 cm^{-1}, 2870 cm^{-1}, 2927 cm^{-1}, 2958cm^{-1}, and 3080 cm^{-1} are ascribed to C=C stretching, – CO – NH – stretching band, symmetric $–CH_2–$ stretching band, asymmetric $–CH_2–$ stretching band, – C – H stretching band, and =C – H stretching band. These results confirm the successful coating of BSA with DPA loading.

The luminous performance of obtained PBMO nanoprobe remains consistent with the ZnGeO:Mn-OH PLNR. PBMO shows a relatively narrow absorption at 250 nm (Fig. 1E, line a). The excitation and emission maxima of PBMO in the luminous spectra are 250 and 530 nm, respectively (Fig. 1E, lines b and c). The luminous decay profiles of PBMO are illustrated in Fig. 1F, and its lifetime is deduced to be 13.21 ms using a two-exponential distribution.

Mechanism of H_2O_2 detection

It is proved by initial experiments that the luminous intensity of ZnGeO:Mn-OH PLNR is not affected by H_2O_2. After coating with BSA, Mn(II), and OPD, the TRF of PBMO can be significantly enhanced under the addition of H_2O_2. In order to explore the response mechanism, PBMO is developed from different concentrations of $Mn(NO_3)_2$ and OPD and their response to 5 μmol L^{-1} H_2O_2 is investigated. When only 2 mol L^{-1} OPD is used, the afterglow luminescence of

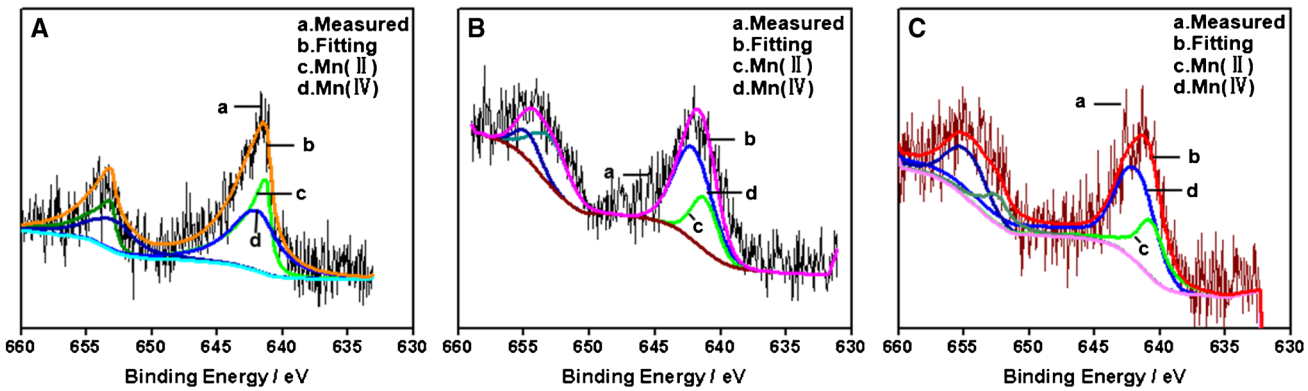

Fig. 3 The high-resolution XPS spectra of Mn 2p in PBMO with OPD (**A**), after adding H_2O_2 (**B**), and without OPD (**C**)

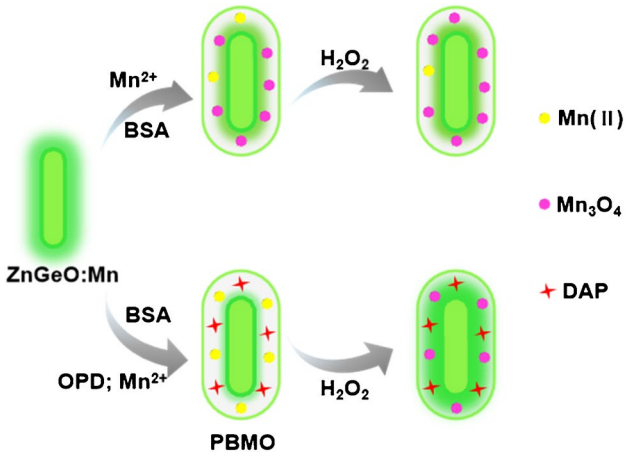

Scheme 1 Schematic illustration of detection mechanism for H_2O_2 by the PBMO nanoprobe

PBMO is the strongest and has no response to H_2O_2. The luminous enhancement efficiency increases with increasing concentration of $Mn(NO_3)_2$ and the strongest signal is obtained at 50 mmol L^{-1} $Mn(NO_3)_2$ (Fig. 2A). Since the generation of precipitation, the luminous enhancement efficiency decreased upon further $Mn(NO_3)_2$ concentration.

However, the afterglow luminescence of PBMO prepared from raw materials that contained only 50 mmol L^{-1} $Mn(NO_3)_2$ can be enhanced by H_2O_2. The luminous enhancement efficiency firstly increases with the OPD concentration in the range of 0 – 2 mol L^{-1}, and then levels off are observed when the OPD concentration is higher than 2 mol L^{-1} (Fig. 2B). The possible reason for this phenomenon is that the BSA shell is saturated with OPD.

Combining with the abovementioned experimental results, we suppose that the main contribution to H_2O_2 response is manganese species. In the presence of $Mn(NO_3)_2$, amorphous $Mn(OH)_2$ is obtained after adding NaOH solution with high concentration, and $Mn(OH)_2$ subsequently transforms into Mn_3O_4 by the oxidation of oxygen dissolved in solution [29]. Then a part of Mn_3O_4 is further reduced to Mn(II) by OPD, which is verified through the peak at 641.0 eV in the high-resolution XPS spectra of Mn 2p. The rest of Mn_3O_4 is further oxidized into Mn(IV) by O_2 under heated condition, which is verified through the peak at 641.9 eV in the high-resolution XPS spectra of Mn 2p (Fig. 3A). The treatment with H_2O_2 possibly leads to oxidation of the Mn(II) in BSA shell under an alkaline condition, inducing the production of Mn_3O_4 and the weaker quenching of luminous intensity. This hypothesis is proved by Fig. 3B, in which the ratio of oxidation state is higher. When no OPD exists, the percentage of Mn(II) in PBMO is decreased from 48 to 30% and the response to H_2O_2 is barely noticeable (Fig. 3C). Thus, the detection mechanism is shown in Scheme 1.

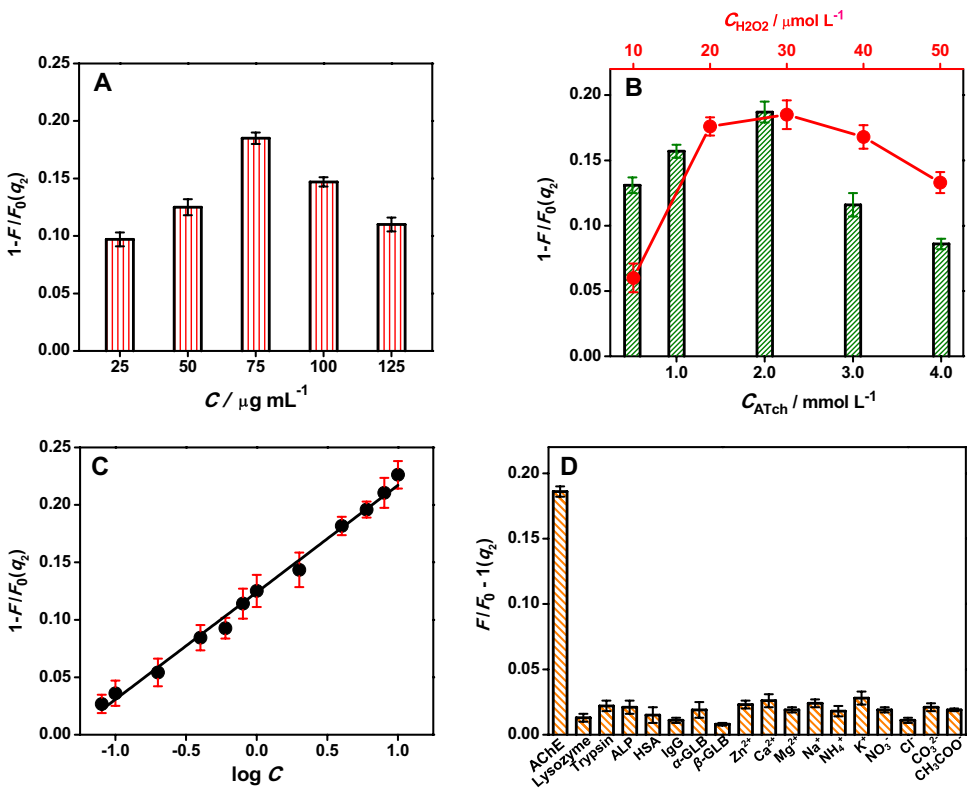

Fig. 4 Effect of PBMO concentration (**A**), and ATch, H_2O_2 concentration (**B**) on AChE detection (AChE concentration: 1.0 U L^{-1}). (**C**) The relationship between the fluorescence quenching efficiency (q_2) and the logarithm of AChE concentration (0.08–10 U L^{-1}). (**D**) Fluorescence response of the proposed probe toward various biomolecules and ions (the concentrations of AChE, enzymes, other proteins, and ions are 1 U L^{-1}, 1 U L^{-1}, 10 μg mL^{-1}, 100 mmol $L.^{-1}$)

Table 1 Comparisons on the performances of this probe with various fluorescent sensors for AChE detection

Fluorescence sensor	Linear range (U L^{-1})	LOD (U L^{-1})	Refs
CdS quantum dots	1 – 10	-	[30]
Carbon nitride quantum dots integrating with phenylboronic acid and alizarin red S	0.5 – 15	0.36	[31]
Polyethyleneimine-protected copper nanoclusters	3 – 200	1.38	[32]
Small molecule fluorescent probe BDFA	4.5 – 1000	4.5	[33]
A near-infrared fluorescent probe containing fluorophore and 2-thienylformyl chloride	0.6 – 10	0.2	[34]
TRF nanoprobe based on heavy metal ion–modified ZnGeO:Mn luminescence nanorods	0.08 – 10	0.03	This study

TRF determination of H_2O_2

To explore the analytical application of PBMO, its luminescence response to H_2O_2 is studied under optimized conditions. Experimental results show that the TRF intensity of PBMO at 530 nm is significantly enhanced within 30 s after mixing with H_2O_2 solutions of different concentrations. As shown in Fig. S2A, the luminous enhancing efficiency (q_1) is linearly proportional to the logarithm of H_2O_2 concentration in the range of 0.4–10 μmol L^{-1}, with a regression equation of $q_1 = 0.326\log C + 0.175$ ($R = 0.995$). The detection limit to H_2O_2 is estimated to be 0.14 μmol L^{-1} from the ratio of triple standard deviation of blank signal to the slope of calibration plot ($3\sigma/s$, n = 11). The successful determination of H_2O_2 by PBMO paves the way for the detection of substances related to H_2O_2.

Analytical performances to AChE

As the key enzyme of biological nerve conduction, AChE can hydrolyze ATCh into TCh. The mercapto group of TCh gives it reducibility, and easily oxidized by H_2O_2. Therefore, we assume that the AChE activity can be detected using the inhibition of TCh to H_2O_2-triggering TRF enhancement. The feasibility of using PBMO nanoprobe to the determination of AChE is verified by recording the TRF intensity under different conditions. The ATCh or AChE has no obvious influence on H_2O_2-triggering TRF enhancement. However, after incubating ATch with AChE and adding H_2O_2, the luminous enhancement efficiency of PBMO is significantly decreased compared to H_2O_2-triggering TRF (line e in Fig. 1E). The experimental parameters affecting AChE detection, for example, the dosage of PBMO, ATCh, and H_2O_2, are thoroughly investigated (Fig. 4A and B). As a result, the optimized concentrations of PBMO, ATCh, and H_2O_2 are 75 μg mL^{-1}, 2 mmol L^{-1}, and 30 μmol L^{-1}.

Experimental results show that the TRF intensity at 530 nm decreases gradually with increasing AChE concentrations in the range of 0.08–10 U L^{-1}. The plots of luminous quenching efficiency (q_2) and the logarithm of AChE concentration possess good linear relationships, with a calibration plot of $q_2 = 0.0931\log C + 0.124$ ($R = 0.997$) (Fig. 4C). The detection limit is calculated to be as low as 0.03 U L^{-1} based on the $3\sigma/s$ rule. The relative standard deviations (RSDs) of intra-day and inter-day are derived to be 2.3% and 4.8%, respectively.

The linearity range and the detection limit (LOD) of this proposed TRF method are compared to those of the previously reported methods for AChE determination (Table 1). The probe we proposed possesses obvious advantages, including high sensitivity, short response time, and easy to operate. To inspect the selectivity of this proposed PBMO nanoprobe, the intensity change of TRF in the presence of potential interfering substances in human serums are measured, including enzymes (lysozyme, trypsin, ALP), proteins with high abundance (HSA, IgG, α-GLB, β-GLB), and ions (Zn^{2+}, Ca^{2+}, Mg^{2+}, Na^+, NH_4^+, K^+, NO_3^-, Cl^-, CO_3^{2-}, CO_3COO^-). Figure 4D shows that these mentioned interfering substances do not pose any interference on the luminescence of PBMO nanoprobe, indicating the excellent detection selectivity of this proposed sensor toward AChE.

Table 2 Determination of AChE contents in real samples ($n = 3$, at 95% confidence level)

Sample	Spiked (U L^{-1})	Found (U L^{-1})	Recovery/%
Diluted serum 1	0	1.30 ± 0.09	-
	4	5.49 ± 0.21	103.6 ± 4.1
	5	6.06 ± 0.26	96.2 ± 4.9
	6	7.21 ± 0.19	98.8 ± 2.7
Diluted serum 2	0	1.51 ± 0.07	-
	4	5.33 ± 0.28	96.7 ± 3.9
	5	6.39 ± 0.21	98.2 ± 2.5
	6	7.55 ± 0.29	100.5 ± 4.0
Diluted serum 3	0	1.09 ± 0.06	-
	4	5.21 ± 0.30	102.4 ± 2.1
	5	5.99 ± 0.21	98.4 ± 1.8
	6	6.87 ± 0.19	96.9 ± 3.4

Analysis of AChE in real samples

To evaluate the practical applicability of this PBMO nanoprobe to real samples, AChE content in human serums is detected. The Cys and GSH in human serum have interference in the AChE detection; thus, a thiolblocking reagent, NEM, is added into human serum [35].

It is found that the AChE concentrations presented in the diluted human serums from healthy volunteers are 1.30 ± 0.09, 1.51 ± 0.07, and 1.09 ± 0.06 U L^{-1} (Table 2), with RSDs of 2.5%, 3.2%, and 2.9%. The spiking standard recovery method is used to evaluate the accuracy of this probe. The spiking recoveries for human serums samples are in the range of 96.2 – 103.6%, implying the potential of this PBMO nanoprobe in analyzing complex samples.

Conclusion

We have established a PBMO nanoprobe for AChE analysis by modifying ZnGeO:Mn PLNR with BSA combined with Mn(II) and OPD. The specific reaction between Mn(II) and H_2O_2 remarkably induces the fluorescence enhancing of PBMO. The outstanding long afterglow luminescence of ZnGeO:Mn PLNR, high fluorescence quenching efficiency of Mn(II), and short distance between energy donor and energy receptor provide the basis for high-sensitive and rapid TRF detection of H_2O_2. Acetylcholinesterase can catalyze ACh to produce TCh, and TCh can easily be oxidized by H_2O_2. The PBMO nanoprobe was successfully applied for the determination of AChE in human serum with much simpler and higher sensitivity. This approach may open a new way to design and apply PLNR-based probes. In addition, this PBMO nanoprobe developed in our study can be employed for other analytes related to H_2O_2.

Supplementary Information The online version contains supplementary material available at https://doi.org/10.1007/s00216-023-05007-9.

Acknowledgements The authors appreciate financial support from the Scientific Research Project of Hainan Provincial Higher Education Institutions (Hnky2023-29), the Initiation Fund for Talents Introduction in Hainan Medical University (RZ2300004368, RZ2300005970), and the High-level Talents Project of Hainan Provincial Natural Science Foundation (220RC617).

Declarations

Ethics approval This study has been approved by the Ethics Committee of Hainan Medical University.

Conflict of interest The authors declare no competing interests.

References

1. Silman I, Sussman JL. Acetylcholinesterase: how is structure related to function? Chem Biol Interact. 2008;175:3–10.
2. Paraoanu LE, Layer PG. Acetylcholinesterase in cell adhesion, neurite growth and network formation. FEBS J. 2008;275(4):618–24.
3. Steinritz D, Emmler J, Hintz M, Worek F, Kreppel H, Szinicz L, Kehe K. Apoptosis in sulfur mustard treated A549 cell cultures. Life Sci. 2007;80:2199–201.
4. Zhang B, Yang L, Yu LY, Lin B, Hou YN, Wu J, Huang Q, Han YF, Guo LH, Ouyang Q, Zhang B, Lu L, Zhang XJ. Acetylcholinesterase is associated with apoptosis in cells and contributes to insulin-dependent diabetes mellitus pathogenesis. Acta Biochim Biophy Sin. 2012;44(3):207–16.
5. Campanari ML, Navarrete F, Ginsberg SD, Manzanares J, Saez-Valero J, Garcia-Ayllon MS. Increased expression of readthrough acetylcholinesterase variants in the brains of Alzheimer's disease patients. J Alzheimers Dis. 2016;53(3):831–41.
6. Subramaniam R, Astot C, Juhlin L, Nilsson C, Ostin A. Direct derivatization and rapid GC-MS screening of nerve agent markers in aqueous samples. Anal Chem. 2010;82(17):7452–9.
7. Liang P, Kang CY, Yang EJ, Ge XX, Du D, Lin YH. A sensitive magnetic nanoparticle-based immunoassay of phosphorylated acetylcholinesterase using protein cage templated lead phosphate for signal amplification with graphite furnace atomic absorption spectrometry detection. Analyst. 2016;141(7):2278–83.
8. Ye C, Wang MQ, Zhong X, Chen S, Chai Y, Yuan R. Highly sensitive electrochemiluminescenc assay of acetylcholinesterase activity based on dual biomarkers using Pd-Au nanowires as immobilization platform. Biosens Bioelectron. 2016;79:34–40.
9. Zhang JJ, Zheng WS, Jiang XY. Ag^+-gated surface chemistry of gold nanoparticles and colorimetric detection of acetylcholinesterase. Small. 2018;14(31):1801680.
10. Xiao T, Wang S, Yan MX, Huang JS, Yang XR. A thiamine-triggered fluormetric assay for acetylcholinesterase activity and inhibitor screening based on oxidase-like activity of MnO_2 nanosheets. Talanta. 2021;221:121362.
11. Guo ZQ, Park S, Yoon J, Shin I. Recent progress in the development of near-infrared fluorescent probes for bioimaging applications. Chem Soc Rev. 2014;43(1):16–29.
12 Suhling K, French PMW, Phillips D. Time-resolved fluorescence microscopy. Photoch Photobio Sci. 2005;4(1):13–22.
13. Deng QS, Zhu Z, Shu XW. Auto-phase-locked time-resolved luminescence detection: principles, applications, and prospects. Front Chem. 2020;8:562.
14. Yuan JL, Wang GL. Lanthanide-based luminescence probes and time-resolved luminescence bioassays. Trends Anal Chem. 2006;25(5):490–500.
15. Liang L, Chen N, Jia YY, Ma QQ, Wang J, Yuan Q, Tan WH. Recent progress in engineering near-infrared persistent luminescence nanoprobes for time-resolved biosensing/bioimaging. Nano Res. 2019;12(6):1279–92.
16. Zhao X, Chen LJ, Zhao KC, Liu YS, Liu JL, Yan XP. Autofluorescence-free chemo/biosensing in complex matrixes based on persistent luminescence nanoparticles. Trends Anal Chem. 2019;118:65–72.
17. Wu SQ, Li Y, Ding WH, Xu LT, Ma Y, Zhang LB. Recent advances of persistent luminescence nanoparticles in bioapplications. Nanomicro Lett. 2020;12(1):1–26.

18. Wu BY, Wang HF, Chen JT, Yan XP. Fluorescence resonance energy transfer inhibition assay for alpha-fetoprotein excreted during cancer cell growth using functionalized persistent luminescence nanoparticles. J Am Chem Soc. 2011;133(4):686–8.
19. Li Y, Gecevicius M, Qiu JR. Long persistent phosphors-from fundamentals to applications. Chem Soc Rev. 2016;45(8):2090–136.
20. Tang YR, Song HJ, Su YY, Lv Y. Turn-on persistent luminescence probe based on graphitic carbon nitride for imaging detection of biothiols in biological fluids. Anal Chem. 2013;85(24):11876–84.
21. Liang T, Li Z, Song D, Shen L, Zhuang QG, Liu ZH. Modulating the luminescence of upconversion nanoparticles with heavy metal ions: a new strategy for probe design. Anal Chem. 2016;88(20):9989–95.
22. Feng Y, Zhang LC, Liu R, Lv Y. Modulating near-infrared persistent luminescence of core-shell nanoplatform for imaging of glutathione in tumor mouse model. Biosens Bioelectron. 2019;144:111671.
23. Feng Y, Song HJ, Deng DY, Lv Y. Engineering ratiometric persistent luminous sensor arrays for biothiols identification. Anal Chem. 2020;92(9):6645–53.
24. Ye QX, Ren SF, Huang H, Duan GG, Liu KM, Liu JB. Fluorescent and colorimetric sensors based on the oxidation of o-phenylenediamine. ACS Omega. 2020;5:20698–706.
25. Chen M, Kutsanedzie FYH, Cheng W, Agyekum AA, Li HH, Chen QS. A nanosystem composed of upconversion nanoparticles and N, N-diethyl-p-phenylenediamine for fluorimetric determination of ferric ion. Microchim Acta. 2018;185(378):1–8.
26. Gao LF, Zhang X, Yang RL, Lv ZW, Yang WG, Hu YH, Zhou B. Time-resolved fluorescence determination of albumin using ZnGeO: Mn luminescence nanorods modified with polydopamine nanoparticles. Microchim Acta. 2021;188(12):429.
27. Wu SQ, Qian ZH, Li Y, Hu SP, Ma Y, Wei SY, Zhang LB. Persistent luminescence nanoplatform with Fenton-like catalytic activity for tumor multimodal imaging and photoenhanced combination therapy. ACS Appl Mater Interfaces. 2020;12(23):25572–80.
28. Wang YQ, Li ZH, Lin QS, Wei YR, Wang J, Li YX, Yang RH, Yuan Q. Highly sensitive detection of bladder cancer-related miRNA in urine using time-gated luminescent biochip. ACS Sens. 2019;4(8):2124–30.
29. Moon J, Awano M, Takai H, Fujishiro Y. Synthesis of nanocrystalline manganese oxide powders: influence of hydrogen peroxide on particle characteristics. J Mater Res. 1999;14(12):4594–601.
30. Liu SR, Chang CY, Wu SP. A fluorescence turn-on probe for cysteine and homocysteine based on thiol-triggered benzothiazolidine ring formation. Anal Chim Acta. 2014;849:64–9.
31. Garai-Ibabe G, Saa L, Pavlov V. Thiocholine mediated stabilization of in situ produced CdS quantum dots: application for the detection of acetylcholinesterase activity and inhibitors. Analyst. 2014;139(1):280–4.
32. Li YY, Liang HB, Lin BX, Yu Y, Wang YM, Zhang L, Cao YJ, Guo ML. A ratiometric fluorescence strategy based on inner filter effect for Cu^{2+}-mediated detection of acetylcholinesterase. Microchim Acta. 2021;188(11):385.
33. Yang JL, Song NZ, Lv XJ, Jia Q. UV-light-induced synthesis of PEI-CuNCs based on Cu^{2+}-quenched fluorescence turn-on assay for sensitive detection of biothiols, acetylcholinesterase activity and inhibitor. Sensor Actuat B Chem. 2018;259:226–32.
34. Yao M, Nie HL, Yao WX, Yang XP, Zhang GW. A sensitive and selective fluorescent probe for acetylcholinesterase: synthesis, performance, mechanism and application. Arabian J Chem. 2022;15(7):103929.
35. Zhao C, Zhou FY, Lu K, Yang SK, Tan BJ, Sun WL, Shangguan LA, Wang HY, Liu Y. Near-infrared fluorescent probe for in vivo monitoring acetylcholinesterase activity. Sensor Actuat B Chem. 2022;360:131647.

Lifang Gao is currently Assistant Research Fellow at Hainan Medical University, China. She was awarded a PhD degree by Northeastern University (China) in 2020. Her work is devoted to the construction of nanometer material–based sensors and their applications in biological assays.

Rong Chen is currently Professor at Hainan Medical University, China. She received her Ph.D. degree from Tsinghua University. Her research interests are the green synthesis of nanomaterials and their biomedical applications.

Haixia Li became Professor of Chemistry at Hainan Medical University, China, in December 2016. She is interested in the modification and design of microporous and mesoporous materials with the aim of improving the analysis performance for small molecules, including antibiotics, metal ions, and glucose.

Dan Xu is currently Associate Professor at Hainan Medical University, China. She received her Ph.D. degree from Jilin University. Her research interests are now focused on the design and synthesis of atomic-scale materials.

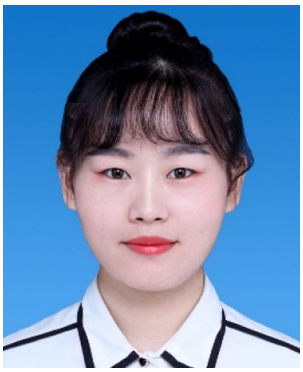

Danning Zheng is currently Lecturer at Hainan Medical University, China. She was awarded a PhD degree by Henan University in 2021. Her current research interests focus on chemical theoretical calculations for catalytic reactions of ionic liquids and probe design.